A novel selective inverse agonist of the CB2 receptor as a radiolabeled tool compound for kinetic binding studies

Martella, A.; Sijben, H.J.; Rufer, A.C.; Grether, U.; Fingerle, J.; Ullmer, C.; ... ; Sijben, H.

1521-0111/92/4/389–400$25.00
MOLECULAR PHARMACOLOGY

https://doi.org/10.1124/mol.117.108605
Mol Pharmacol 92:389–400, October 2017

A Novel Selective Inverse Agonist of the CB_2 Receptor as a Radiolabeled Tool Compound for Kinetic Binding Studies

Andrea Martella, Huub Sijben, Arne C. Rufer, Uwe Grether, Juergen Fingerle, Christoph Ullmer, Thomas Hartung, Adriaan P. IJzerman, Mario van der Stelt, and Laura H. Heitman

Division of Medicinal Chemistry, Leiden Academic Centre for Drug Research (A.M., H.S., A.P.I., L.H.H.), and Department of Molecular Physiology, Leiden Institute of Chemistry (A.M., M.S.), Leiden University, Leiden, The Netherlands; Roche Pharma Research and Early Development, Roche Innovation Center Basel, F. Hoffmann-La Roche Ltd., Basel, Switzerland (A.M., A.C.R., U.G., C.U., T.H.); and Natural and Medical Sciences Institute, University of Tübingen, Reutlingen, Germany (J.F.)

Received February 16, 2017; accepted July 21, 2017

ABSTRACT

The endocannabinoid system, and in particular the cannabinoid type 2 receptor (CB2R), raised the interest of many medicinal chemistry programs for its therapeutic relevance in several (patho)-physiologic processes. However, the physico-chemical properties of tool compounds for CB2R (e.g., the radioligand [^{3}H]CP55,940) are not optimal, despite the research efforts in developing effective drugs to target this system. At the same time, the importance of drug-target binding kinetics is growing since the kinetic binding profile of a ligand may provide important insights for the resulting in vivo efficacy. In this context we synthesized and characterized [^{3}H]RO6957022, a highly selective CB2R inverse agonist, as a radiolabeled tool compound. In equilibrium and kinetic binding experiments [^{3}H]RO6957022 showed high affinity for human CB2R with fast association (k_{on}) and moderate dissociation (k_{off}) kinetics. To demonstrate the robustness of [^{3}H]RO6957022 binding, affinity studies were carried out for a wide range of CB2R reference ligands, spanning the range of full, partial, and inverse agonists. Finally, we used [^{3}H]RO6957022 to study the kinetic binding profiles (i.e., k_{on} and k_{off} values) of selected synthetic and endogenous (i.e., 2-arachidonoylglycerol, anandamide, and noladin ether) CB2R ligands by competition association experiments. All tested ligands, and in particular the endocannabinoids, displayed distinct kinetic profiles, shedding more light on their mechanism of action and the importance of association rates in the determination of CB2R affinity. Altogether, this study shows that the use of a novel tool compound, i.e., [^{3}H]RO6957022, can support the development of novel ligands with a repertoire of kinetic binding profiles for CB2R.

Introduction

Historically, the plant *Cannabis sativa* and its preparations have been exploited for millennia, finding its use in medical and recreational applications (Mechoulam et al., 2014). Since the structural characterization of Δ^9-tetrahydrocannabinol, the main psychoactive constituent of cannabis, in 1964 (Gaoni and Mechoulam, 1964) two class A, G protein-coupled receptors were identified as a target of Δ^9-tetrahydrocannabinol, namely, the cannabinoid type 1 receptor (Devane et al., 1988) and the cannabinoid type 2 receptor (CB2R) (Munro et al., 1993). The presence of these G protein-coupled receptors implied the existence of endogenous ligands, which were identified as signaling lipids derived from arachidonic acid, i.e., anandamide [*N*-arachidonoylethanolamine (AEA)] and 2-arachidonoylglycerol (2-AG). These bioactive lipids were coined endocannabinoids (Di Marzo and Fontana, 1995). More recently, complete enzymatic machinery was found to control the levels of these endocannabinoids, which are synthetized and degraded in an on-demand fashion after various types of stimuli (Ligresti et al., 2016).

The two cannabinoid receptors are expressed in different cellular systems throughout the human body and are involved in various physiologic and pathologic processes. Cannabinoid receptor type 1 is mainly expressed in the central nervous system and to a lesser extent in peripheral tissue, whereas the CB2R is thought to be primarily expressed in immune cells (e.g., B and T lymphocytes, monocytes, and macrophages) (Galiègue et al., 1995; Turcotte et al., 2016).

Since its discovery, CB2R has become an interesting anti-inflammatory target in a variety of disease areas (Dhopeshwarkar and Mackie, 2014; Picone and Kendall, 2015), including pain (Guindon and Hohmann, 2008; Anand et al., 2009), neurologic disorders (e.g., Parkinson's disease and Huntington's chorea) (Cabral et al., 2008; Fernández-Ruiz et al., 2011; Aso et al., 2013), osteoporosis (Ofek et al., 2006), nephropathy (Mukhopadhyay et al., 2010, 2016), hepatic diseases (Lotersztajn et al., 2008), and ischemia reperfusion injury

U.G., C.U., T.H., and A.C.R. are employees of F. Hofmann-La Roche Ltd.
https://doi.org/10.1124/mol.117.108605.
S This article has supplemental material available at molpharm.aspetjournals.org.

ABBREVIATIONS: AEA, anandamide (*N*-arachidonoylethanolamine); 2-AG, 2-arachidonoylglycerol; BSA, bovine serum albumin; CB2R, cannabinoid type 2 receptor; CHO, Chinese hamster ovary; NE, noladin ether; NSB, non-specific binding; PEI, polyethylenimine; RT, residence time; TB, total binding.

(Horváth et al., 2012; Li et al., 2013). Hence, considerable effort has been put into the synthesis and preclinical screening of novel CB2R-selective ligands, where the in vivo application of some of these has already generated some promising results (Riether, 2012; Morales et al., 2016). However, despite these efforts, thus far no CB2R ligands have shown efficacy in clinical trials (Dhopeshwarkar and Mackie, 2014). Poor in vitro characterization of the drug candidates, ambiguous findings in animal models (Moris et al., 2015), and low interspecies CB2R homology (Brown et al., 2002) could have contributed to these failures in clinical trials, and novel approaches are needed to bridge this translational gap (Soethoudt et al., 2017).

A decade ago, the concept of drug-target binding kinetics was introduced as a means to better predict the in vivo efficacy of ligands, in addition to conventional lead optimization parameters such as ligand affinity and potency (Copeland et al., 2006). The concept takes into account the receptor recognition of the ligand, defined by the association rate (k_{on}, in nM^{-1}/min^{-1}) and the ligand-receptor complex stability, defined by the dissociation rate (k_{off}, in min^{-1}). These kinetic parameters hold important information that can be related to a drug's in vivo efficacy. For instance, the residence time (RT), which is defined as the reciprocal of k_{off}, is a measure of the stability of the ligand-receptor complex and has been shown (retrospectively) to correlate with drug efficacy and safety (Tummino and Copeland, 2008). In addition, recent studies outlined the importance of a high k_{on} value as an important determinant to achieve sufficient target occupancy (de Witte et al., 2016) by means of rebinding and micro-pharmacokinetic processes (Sykes et al., 2014; Vauquelin, 2016).

To the best of our knowledge, to date there have been no reports on CB2R ligand binding kinetics. Therefore, applying this novel approach to study the CB2R kinetic binding behavior of endogenous and synthetic ligands could yield important insights in cannabinoid receptor drug research.

With respect to the classic filtration binding assay typically performed with the unselective [^{3}H]CP55,940, kinetic binding experiments require a more robust radiolabeled tool compound with low nonspecific binding (NSB). In this study, we describe the characterization of [^{3}H]RO6957022 (Fig. 1), a novel tritiated compound with nanomolar affinity, inverse agonist behavior, and high selectivity for CB2R (Slavik et al., 2015). This compound is based on a 2,5,6-substituted pyridine scaffold and was previously reported as a positron emission tomography imaging probe in [^{11}C]-labeled form (Slavik et al., 2015). To support its relevance as an in vitro binding kinetics tool compound, we used it to determine the kinetic binding profile of chemically diverse CB2R ligands in the range of full, partial, and inverse agonists. Moreover, this paper describes for the first time the binding kinetics of endocannabinoids on CB2R.

Materials and Methods

Chemicals and Reagents. Bovine serum albumin (BSA), polyethylenimine (PEI), CP55,940, GW405833, AM1241, and AM630 were purchased from Sigma Aldrich (St. Louis, MO). JWH-133, HU-308, AEA, 2-AG, and noladin ether (NE) were supplied by Tocris Bioscience (Bristol, United Kingdom). Bicinchoninic acid protein assay reagent was purchased from Pierce Chemical Co. (Rockford, IL). SR144528 was purchased from Santa Cruz Biotechnology (Dallas, TX). LEI-101 was provided by M. Baggelaar from the Molecular Physiology Group (Leiden Institute of Chemistry, Leiden University). PathHunter β-arrestin Chinese hamster ovary (CHO)-K1 cells stably expressing human CB2R (CHO-K1_hCB$_2$) were purchased from DiscoverX (Fremont, CA). All other chemicals were of analytical grade and obtained from commercial sources.

Cell Culture and Membrane Preparation. CHO-K1_hCB$_2$ cells were cultured in Dulbecco's modified Eagle's media/nutrient F-12 Ham 1:1 mixture (Sigma-Aldrich, St. Louis, MO) supplemented with 10% fetal calf serum (Sigma), 300 μg/ml hygromycin (InvivoGen, San Diego, CA), 800 μg/ml G418 (Duchefa Biochemie, Haarlem, The Netherlands), 100 μg/ml penicillin/streptomycin (Duchefa Biochemie, Haarlem, The Netherlands), and Glutamax (Gibco, Waltham, MA) at 37°C and 5% CO_2. Cells were subcultured twice a week at 90% confluency. Confluent cells were trypsinized and pooled. Subsequently, cells were pelleted and resuspended in ice-cold buffer (50 mM Tris-HCl at pH 7.4) and homogenized using an Ultra Turrax homogenizer (IKA-Werke GmbH & Co. KG, Staufen, Germany). CHO-K1_hCB$_2$ membranes were obtained by a double centrifugation step at 100,000*g* at 4°C for 20 minutes (Optima LE-80K Ultracentrifuge, Beckman Coulter, Brea, United States), after which the suspension was aliquoted and stored at −80°C until further use. Just prior to use membranes were thawed, homogenized using an Ultra Turrax homogenizer and diluted to 60 μg/ml with ice-cold assay buffer (Tris-HCl 50 mM, pH 7.4 and 0.1% BSA). Protein concentrations were determined for each batch of membranes by a bicinchoninic acid protein assay (Smith et al., 1985).

Preparation of [^{3}H]RO6957022. A solution of 870 μg (2.14 μmol) of the *O*-desmethyl precursor 3-ethyl2-(6-(cyclopropylmethoxy)-5-(3-hydroxyazetidin-1-yl)picolinamido)-2-ethylbutanoate and 1.43 μmol of Lithium bis(trimethylsilyl)amide (1 M in Tetrahydrofuran) in 100 μl of Dimethylformamide was added to 50 mCi (1.85 GBq, 0.714 μmol) of [^{3}H]-methyl nosylate in a 1 ml reaction vial. After stirring for 16 hours at room temperature, the reaction mixture was treated with 5 ml of water and extracted three times with 4 ml of Tert-Butyl Methyl Ether. The organic layers were separated, dried over sodium sulfate, and then the solvent was removed in vacuum. The crude product was purified by flash chromatography (silica, AcOEt/*n*-heptane 1:4) to yield 4.2 mCi (8.4%) of the tritium-labeled radioligand in 96.7% radiochemical purity and a specific activity of 83.7 Ci/mmol (3.1 TBq/mmol). Radiochemically highly pure material (>99%) can be obtained by additional high-performance liquid chromatography purification with Waters (GmbH Eschborn, Germany) XBridge C18, acetonitrile/water 30/70 to 90/10 over 20 minutes.

Saturation Binding Experiments With [^{3}H]RO6957022. In the saturation experiments, CHO-K1_hCB$_2$ membranes (1.5 μg per well) were incubated with radioligand in assay buffer (Tris-HCl 50 mM, pH 7.4, and 0.1% BSA) at 25°C for 90 minutes (to ensure equilibrium was reached at all radioligand concentrations). Total binding (TB) was determined by increasing concentrations of [^{3}H]RO6957022 between 0.3 and 18 nM, whereas NSB was determined at three concentrations of radioligand in the presence of AM630 (10 μM). Incubations were terminated by rapid filtration through a 96-well GF/C filter plate using a FilterMate 96-well plate harvester (Perkin-Elmer, Waltham, MA). The GF/C filters were pretreated with 0.25% PEI, 30 minutes prior to harvesting. Subsequently, filters were washed at least three times with ice-cold assay buffer and then completely dried. Remaining radioactivity on the filter was detected by adding 25 μl Microscint scintillation cocktail to each well and counted using a MicroBeta^2 2450 Microplate Counter (Perkin-Elmer). Specific binding was obtained by linear subtraction of NSB from TB. For all of the experiments TB was always <10% of the total amount of radioligand added to prevent ligand depletion. Moreover, [^{3}H]RO6957022 did not significantly bind to the control CHO-K1 membranes.

Displacement Experiments with [^{3}H]RO6957022. In the homologous and heterologous displacement experiments, CHO-K1_hCB$_2$ membranes (1.5 μg per well) were incubated in assay buffer at 25°C

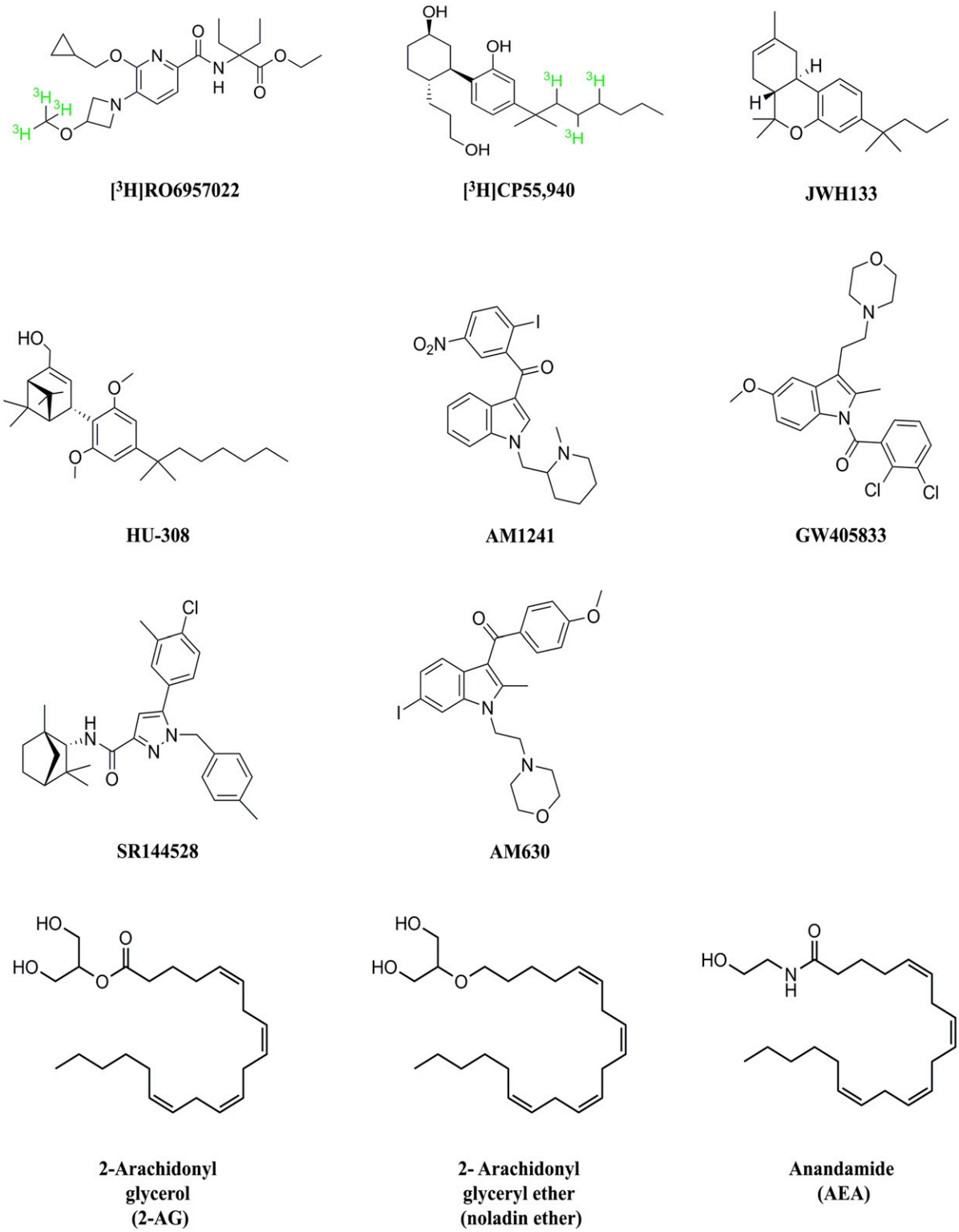

Fig. 1. Chemical structures of the tested CB2R ligands. The present compound selection included synthetic full (i.e., RO6957022, CP55,940, HU-308, and AM1241), partial (i.e., GW405833) and inverse agonists (i.e., SR144528 and AM630), as well as endogenous CB2R ligands (i.e., 2-AG, AEA, and NE).

with a fixed amount of [^{3}H]RO6957022 (3 nM) in the presence of increasing concentrations of unlabeled competing ligand. The dilution series of unlabeled competing ligand were dispensed by a HP D300 digital dispenser (Tecan, Giessen, The Netherlands) and incubated until equilibrium was reached. TB was determined in the presence of buffer and set at 100%, while NSB was determined in the presence of AM630 (10 μM) and set at 0%. Harvesting and counting procedures were performed as described in *Saturation Binding Experiments with [^{3}H]RO6957022*.

Association and Dissociation Experiments with [^{3}H]RO6957022. In the association experiments, CHO-K1_hCB_2 membranes (1.5 μg per well) were incubated in assay buffer at 25°C with a fixed amount of

[^{3}H]RO6957022 (3 nM) at different time points between 0 and 90 minutes. For dissociation experiments, membranes were incubated for 90 minutes in assay buffer at 25°C with a fixed amount of [^{3}H]RO6957022 (3 nM). Subsequently, dissociation of [^{3}H]RO6957022 was initiated by addition of 5 μl of an excess of AM630 (final concentration of 10 μM) to each well at different time points between 0 and 90 minutes. AM630 was chosen as a displacer of its inverse agonist nature and different chemical scaffold with respect to RO6957022. Harvesting and counting procedures were performed as described in *Saturation Binding Experiments with [^{3}H]RO6957022*.

Competition Association Experiments with [^{3}H]RO6957022. The kinetic parameters of unlabeled competitor ligands were determined using the competition association assay as described by Motulsky and Mahan (1984). CHO-K1_hCB$_2$ membranes (1.5 μg per well) were incubated in assay buffer at 25°C with a fixed amount of [^{3}H]RO6957022 (3 nM) at different time points between 0 and 90 minutes in either the absence (control) or presence of an unlabeled competing ligand. Assay validation was performed by homologous competition association, as described in the results section (Fig. 3). The IC$_{50}$ concentrations of the unlabeled competitor ligands were used to obtain approximately 50% displacement of the radioligand after 90 minutes of incubation with [^{3}H]RO6957022. Appropriate vehicle controls [i.e., dimethylsulfoxide, ethanol, and Tocrisolve (Tocris Bioscience)] were used according to the solvent used for each ligand. To prevent degradation of the endocannabinoids during the assay, 1 μM of phenylmethylsulfonyl fluoride was added to membrane preparations 30 minutes in advance of the assay. Harvesting and counting procedures were performed as described in *Saturation Binding Experiments with [^{3}H]RO6957022*.

Data Analysis. All data were analyzed using GraphPad Prism v7.00 for Windows (GraphPad Software, Inc., San Diego, CA). The equations given subsequently were used to analyze the data and fit the curves. Application of the *F* test (Ludden et al., 1994) as implemented for comparison of nested models showed that a monophasic association model described the data sufficiently. When we considered two nested models, in which model 1 corresponded to the simpler model, we applied the following equation: $F = [(SS_1 - SS_2)/(DF_1 - DF_2)]/(SS_2/DF_2)$, where SS is the sum of the squares and DF is the degrees of freedom for each model. For specific saturation binding of [^{3}H]RO6957022, the data were analyzed with the nonlinear regression one site–specific binding model of GraphPad Prism, given by the following equation: $Y = B_{max} \times X/(K_D + X)$, where Y is the specific radioligand binding in pmol/mg protein, B_{max} is the total amount of receptors, X depicts the [^{3}H]RO6957022 concentration in nanomolars, and K_D is the equilibrium affinity constant in nanomolars. For the homologous and heterologous displacement experiments, the data were analyzed with the nonlinear regression one site–fit log IC$_{50}$ model given by the following equation:

$$Y = \text{Bottom} + (\text{Top} - \text{Bottom})/\left(1 + 10^{X - \log IC_{50}}\right),$$

where Y is the specific [^{3}H]RO6957022 binding, Top and Bottom are the plateau values of the curves both in the unit of Y, X represents the unlabeled competitor concentration in log M, and log IC$_{50}$ is the equilibrium affinity of the competing ligand used. Subsequently, the K_i values were calculated using the Cheng-Prusoff equation (Cheng and Prusoff, 1973): $K_i = IC_{50}/(1 + ([L]/K_D)$, where [L] is the [^{3}H]RO6957022 concentration in nanomolars and K_D is the equilibrium affinity value of [^{3}H]RO6957022 in nanomolars. The association rate constants (k_{on}) were determined by the following equation: $k_{on} = (k_{obs} - k_{off})/[L]$, where [L] is the [^{3}H]RO6957022 concentration in nanomolars. The observed association rates (k_{obs}) were determined with a one-phase exponential association analysis: $Y = Y_0 + (\text{Plateau} - Y_0) \times (1 - \exp(-k_{obs} \times t)$, where Y_0 is the specific radioligand binding at time 0, Plateau represents the maximum specific [^{3}H]RO6957022 binding at equilibrium, k_{obs} is the observed association rate in min^{-1}, and t is time in minutes. The dissociation rate constants (k_{off}) were determined with a one-phase exponential decay analysis: $Y = (Y_0 - NSB) \times \exp(-k_{off} \times t) + NSB$, where k_{off} is the dissociation rate constant in min^{-1}. The data from the homologous and heterologous competition association experiments were analyzed by the following equation (Motulsky and Mahan, 1984): $[RL] = (B_{max}\, k_1[L]/K_F - K_S) \times [k_4(K_F - K_S)/(K_F K_S)] + [(k_4 - K_F)/K_F] \times \exp(-K_F t) - [(k_4 - K_S)/K_S] \times \exp(-K_S t)$, using the following variables:

$$K_A = k_1[L] + k_2$$
$$K_B = k_3[I] + k_4$$
$$K_F = 0.5 \times \left(K_A + K_B + \sqrt{\left\{(K_A - K_B)^2 + 4 \times k_1 k_3 [L][I]\right\}}\right)$$
$$K_S = 0.5 \times \left(K_A + K_B - \sqrt{\left\{(K_A - K_B)^2 + 4 \times k_1 k_3 [L][I]\right\}}\right)$$

where [RL] is the amount of receptor-ligand complex; [L] is the concentration [^{3}H]RO6957022 in nanomolars; [I] depicts the concentration of unlabeled competitor in nanomolars; K_A and K_B are the observed association (k_{obs}) of [^{3}H]RO6957022 and the unlabeled competitor, respectively; k_1 and k_3 are the association rate constants (k_{on}) of [^{3}H]RO6957022 and the unlabeled competitor, respectively; k_2 and k_4 are the dissociation rate constants (k_{off}) of [^{3}H]RO6957022 and the unlabeled competitor, respectively; and t is the time in minutes. The receptor RT was calculated by taking the reciprocal of the dissociation rate ($1/k_{off}$) (Copeland et al., 2006). The correlation between two independent variables with the Gaussian distribution was calculated by using the Pearson correlation coefficient (r), with two-tailed P value determination (Benesty et al., 2009).

Results

Assay Binding Optimization of [^{3}H]RO6957022 to the Human CB$_2$ Receptor. Initial experiments were focused on specific [^{3}H]RO6957022 binding to human CB2R and optimizing the assay conditions for in vitro binding studies. Therefore, the presence of several additives were initially tested in a standard assay buffer (50 mM Tris HCl, pH 7.4) together with 3 nM of [^{3}H]RO6957022 and CHO-K1_hCB2 membranes (Fig. 2A). To reduce the NSB of [^{3}H]RO6957022 to the GF/C filters during the harvesting process, the filters were preincubated for 30 minutes with PEI, which resulted in a dramatic decrease in NSB, which was largely caused by filter binding of [^{3}H]RO6957022 (Fig. 2A). We thus concluded that the presence of 0.1% 3-[(3-cholamidopropyl)dimethylammonio]-1-propanesulfonic acid or 0.1% w/v BSA (which we finally selected) in the assay buffer and pretreatment of the filters with 0.25% w/v of PEI was sufficient to provide a signal-to-noise ratio of [^{3}H]RO6957022 binding of sufficient quality. Moreover, receptor specificity was confirmed by comparing the specific binding in CHO-K1_hCB2 versus control CHO cells without overexpressing CB2R (Fig. 2B). Subsequently, membrane titration was performed to assess which concentration yielded an optimal window, i.e., large enough but below the ligand depletion limit (i.e., 10% of the total amount of radioligand present). By using 1.5 μg/well of CHO-K1_hCB$_2$ membranes we obtained approximately 4000 dpm of specific binding. As expected, [^{3}H]RO6957022 specific binding was directly correlated with the concentration of CHO-K1_hCB$_2$ membranes used (Fig. 2C), while NSB was not affected, indicating that this residual binding was indeed mostly caused by the filter.

[^{3}H]RO6957022 Saturation Experiment to the Human CB$_2$ Receptor. To confirm the affinity of [^{3}H]RO6957022 for CB2R, we performed equilibrium saturation binding experiments (Fig. 3A). Binding of [^{3}H]RO6957022 to CHO-K1_hCB$_2$

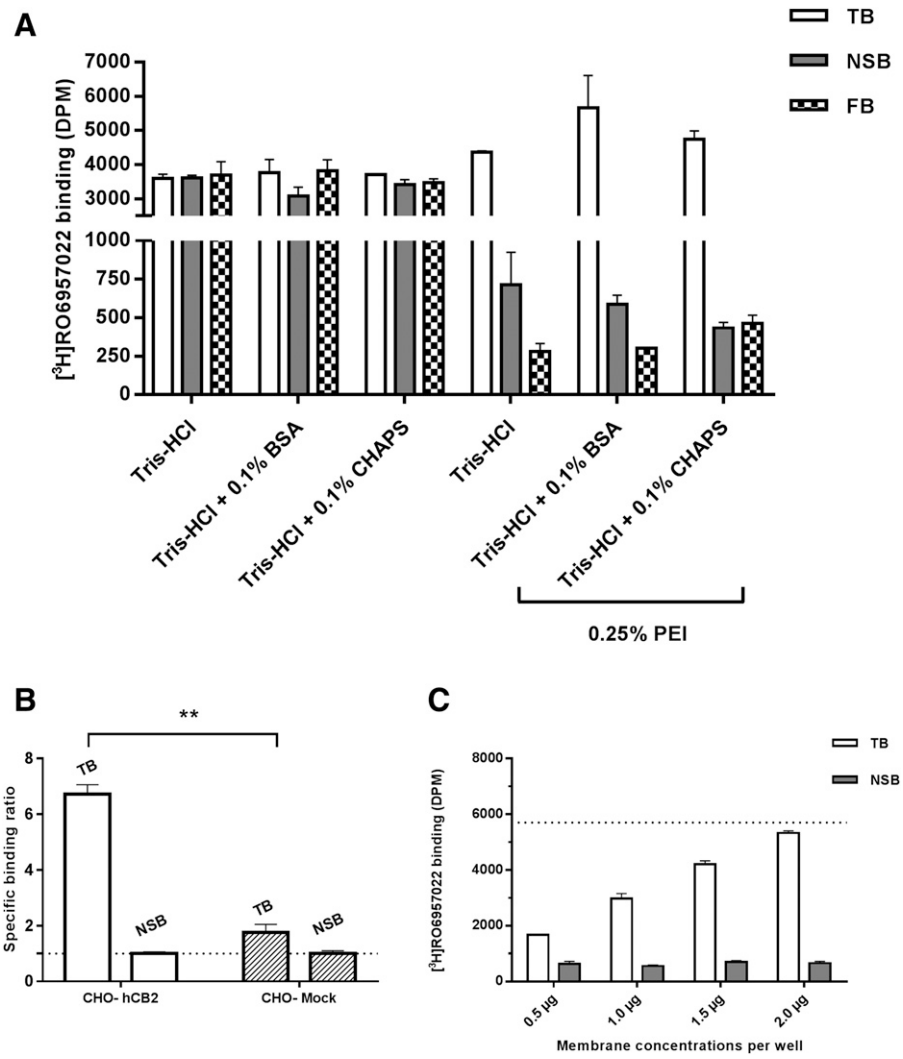

Fig. 2. Binding assay optimization and window determination of [^{3}H]RO6957022 to CHO-K1_hCB_2 membranes. Initially, various assay buffers and filter pretreatments were tested (A) to reduce NSB and filter binding. Once the optimal assay condition was determined (i.e., 50 mM Tris-HCl pH 7.4 and 0.1% BSA and filters prewetted with PEI), receptor specificity was tested comparing TB and NSB using 15 μg membranes from CHOK1_hCB2 and mock control (B). Data are representative of the ratio between TB and NSB (dashed line), statistical comparisons were carried out with an unpaired Student's t test for each experimental group (**$P < 0.01$). Single-point binding experiments were performed to determine the optimal membrane concentration in terms of specific window and ligand depletion limit (dashed line) (C). Data are shown as the mean and S.E.M. from three independent experiments performed in duplicate.

membranes was saturable and best described by a one-site model. The equilibrium dissociation constant (K_D) of [^{3}H]RO6957022 was found to be 1.7 ± 0.1 nM, with a receptor density (B_{max}) value of 25 ± 1 pmol/mg protein in the membranes used (Table 1).

Equilibrium Displacement Assay Using [^{3}H]RO6957022 and CB2R Reference Ligands. Next, [^{3}H]RO6957022 was used to perform displacement experiments with eight previously reported orthosteric CB2R ligands (Fig. 1). These included agonists (CP55,940, JWH-133, AM1241, and HU-308), a partial agonists (GW405833, LEI-101), and inverse agonists (SR144528 and AM630). All compounds tested were able to fully displace [^{3}H]RO6957022 from the orthosteric binding site with nanomolar affinities (Fig. 4; Table 2). In addition, we performed a homologous displacement assay with RO6957022, which resulted in an affinity of 1.3 nM (pK_i = 8.9) for the unlabeled compound, i.e., similar to its equilibrium K_D value determined from [^{3}H]RO6957022 saturation experiments (Fig. 1; Table 1).

Kinetic Characterization of [^{3}H]RO6957022 on the Human CB_2 Receptor. Subsequently, the association (k_{on}) and dissociation (k_{off}) rate constants of [^{3}H]RO6957022 were determined (Fig. 3B; Table 2). The binding of [^{3}H]RO6957022 reached equilibrium after approximately 10 minutes at 25°C. Specific [^{3}H]RO6957022 binding was stable for at least 3 hours (Supplemental Fig. 1) and reversible, since complete dissociation was achieved within 60 minutes upon addition of 10 μM of AM630 (Fig. 3B). From the association and dissociation curves, the k_{on} value was determined to be 0.11 ± 0.01 nM^{-1}/min^1, while the k_{off} value was determined to be 0.16 ± 0.01 min^{-1}, respectively. The latter resulted in a RT of 6.3 ± 0.5 minutes (Table 1). Using the obtained k_{on} and k_{off} values, the kinetic K_D value was determined to be 1.4 nM, which was in agreement with the equilibrium K_D and K_i values obtained from the saturation and homologous displacement experiments, respectively.

[^{3}H]RO6957022 Homologous Competition Association. With the k_{on} (k_1) and k_{off} (k_2) values of [^{3}H]RO6957022 already quantified, the k_{on} (k_3) and k_{off} (k_4) values for unlabeled RO6957022 were determined by performing homologous competition association experiments as a validation step (Fig. 5). For this purpose, three different concentrations of RO6957022 were used to compete with [^{3}H]RO6957022 (i.e., 1, 3, and 9 nM), which corresponded to 0.3-, 1.0-, and 3.0-fold IC_{50} concentrations, respectively. This resulted in k_{on} (k_3) and k_{off} (k_4) values for unlabeled RO6957022 of 0.13 ± 0.03 nM^{-1}/min^{-1} and 0.18 ± 0.01 min^{-1}, respectively (Table 2). Comparison of these values, as well as the calculated kinetic K_D and the other equilibrium and kinetic parameters obtained (Table 2), confirmed the accuracy of the [^{3}H]RO6957022 competition

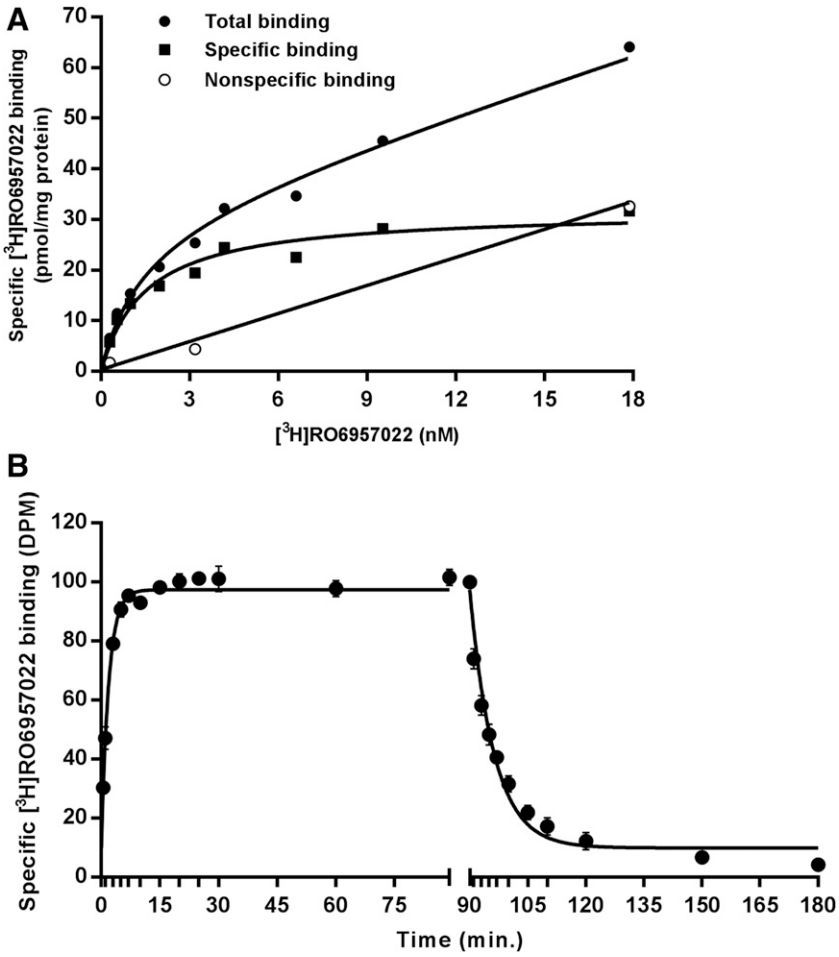

Fig. 3. Equilibrium and kinetic characterization of [^{3}H]RO6957022 binding. (A) Representative saturation binding experiment of [^{3}H]RO6957022 in either the absence (closed circles) or presence (open circles) of 10 μM AM630 to determine NSB. (B) Association and dissociation experiment with 3 nM [^{3}H]RO6957022 interacting with CHO-K1_hCB$_2$ membranes at 25°C. Dissociation of the radioligand was initiated by addition of 10 μM AM630 (final concentration) after equilibrium had been reached. Association and dissociation rate constants were best fitted using a one-phase association or dissociation model, where data are represented as the mean and S.E.M. of six independent experiments performed in duplicate.

association assay to determine the kinetics of unlabeled competitors at the CB2R. As proof of concept, the obtained kinetic parameters derived from the shared analysis in the presence of three concentrations of RO6957022 were compared with the k_3 and k_4 values determined with a single concentration (i.e., 1.0-fold IC_{50}). Comparable values were achieved with only one concentration of competing unlabeled ligand (Table 2); therefore, a similar approach was also applied for the susbsequent kinetic binding studies of other unlabeled competitors.

TABLE 1
Affinity and kinetic binding properties of [^{3}H]RO6957022 as determined by various assay types

Binding Assay	k_{on} (nM^{-1}/min^{-1})	k_{off} (min^{-1})	RT (minute)	K_D, K_i (nM)	B_{max} (pmol/mg protein)
Association[a]	0.11 ± 0.01	—	—	—	—
Dissociation[b]	—	0.16 ± 0.01	6.3 ± 0.5	1.4 ± 0.2	—
Competition association (three concentrations)[c]	0.13 ± 0.03	0.18 ± 0.01	5.5 ± 0.3	1.4 ± 0.3	—
Competition association (one concentration)[d]	0.15 ± 0.03	0.19 ± 0.03	5.3 ± 0.7	1.3 ± 0.4	—
Saturation[e]	—	—	—	1.7 ± 0.1	25 ± 1
Displacement[f]	—	—	—	1.3 ± 0.1	—

[a]Association rate constants as determined with [^{3}H]RO6957022 (for corresponding graph see Fig. 3B).
[b]Dissociation rate constants as determined with [^{3}H]RO6957022 (for corresponding graph see Fig. 3B).
[c]Competition association with three concentrations (0.3-, 1.0-, and 3.0-fold IC_{50}) of cold RO6957022 (for corresponding graph see Fig. 4); $K_D = k_{off}/k_{on}$.
[d]Competition association with a single concentration (1.0-fold IC_{50}) of cold RO6957022 (for corresponding graph see Fig. 4); $K_D = k_{off}/k_{on}$.
[e]The K_D value obtained from saturation binding of [^{3}H]RO6957022 (for corresponding graph see Fig. 3A).
[f]The K_i value obtained from homologous displacement of cold RO6957022 by [^{3}H]RO6957022 (for corresponding graph see Fig. 4).
Data shown are presented as the mean ± S.E.M. of at least three individual experiments, em dashes indicate the absence of value for the corresponding assay.

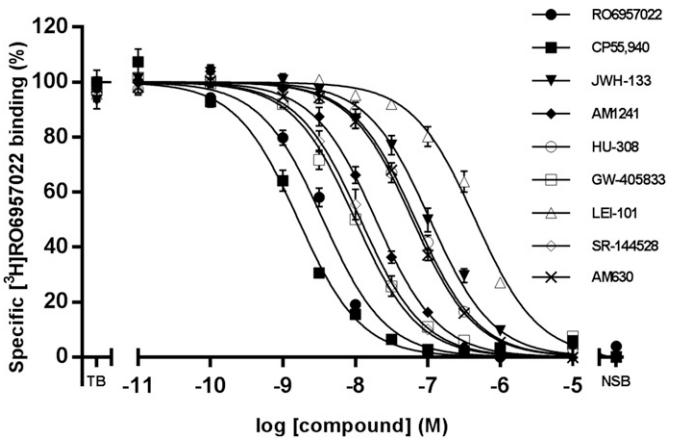

Fig. 4. Binding affinity determination of reference CB_2 ligands using [^{3}H]RO6957022. Heterologous displacement experiments on CHO-K1_hCB_2 membranes using a selection of CB_2 full (CP55,940; JWH-133, AM1241, and HU-308), partial (GW405833, LEI-101), and inverse (SR144528 and AM630) agonists, including homologous displacement of [^{3}H]RO6957022. Data are shown as the mean and S.E.M. of three independent displacement experiments each performed in duplicate.

Kinetic Binding Profile Determination of Known Synthetic CB_2 Ligands. Using the validated [^{3}H]RO6957022 competition association assay, five of the eight CB2R ligands that were tested in a displacement assay (CP55,940, JWH-133, HU-308, GW405833, and SR144528) were selected to assess their kinetic binding profile (Fig. 6). [^{3}H]RO6957022 association was challenged with 1.0-fold IC_{50} concentration of a competitor and typical competition association graphs were obtained (Fig. 6). By fitting the kinetic binding parameters of [^{3}H]RO6957022 in the model (Motulsky and Mahan, 1984), we were able to calculate the association and dissociation rate constants for all tested CB2R ligands (Table 2). All full and partial agonists displayed dissociation kinetics at CB2R with high k_{off} values and thus a short RT; the latter was reflected by a typical shallow association curve in the presence of a quickly dissociating competitor. However, the association rate constants of the synthetic agonists differed up to approximately 60-fold, to the extent that CP55,940 and GW405883 associated to CB2R faster and JWH-133 was the slowest to associate. Interestingly, the association curve obtained in the presence of SR144528, a CB2R inverse agonist, showed a characteristic overshoot, indicating a slower dissociation of SR144528 from the receptor relative to [^{3}H]RO6957022 (k_{off} = 0.12 ± 0.02 min^{-1} versus k_{off} = 0.19 ± 0.03 min^{-1}, respectively).

Kinetic Binding Profile of Endocannabinoids and Noladin Ether. Finally, we assessed the binding kinetics of the two major endocannabinoids on CB2R (Fig. 1), AEA and 2-AG, as well as a proposed endocannabinoid, NE. In competition association experiments with [^{3}H]RO6957022, the three endocannabinoids displayed a distinct kinetic profile. As for the synthetic agonists, the dissociation rate constants displayed moderate differences with AEA having the highest RT of 1.4 minutes, followed by 2-AG and NE with 0.31 and 0.16 minutes, respectively (Fig. 7; Table 2). In contrast and similar to the synthetic agonists, the endocannabinoid-receptor association rates were quite different, where 2-AG and NE had more than 10-fold higher k_{on} values than AEA.

Correlation Plots. Considering that the affinity of a ligand is a function of its k_{on} and k_{off} values for a target, all of the derived kinetic target affinities were compared with the corresponding equilibrium affinity values obtained with the heterologous displacement experiments (Fig. 8A). A strong correlation (r = 0.984, $P < 0.0001$) between the negative logarithm of equilibrium affinity values (pK_i) and the kinetic affinity (pK_D) values of all tested ligands was observed. Similarly, we plotted the k_{on} (Fig. 8B) and k_{off} (Fig. 8C) values against the corresponding ligand affinities, where a significant positive correlation was found between the k_{on} and affinity values (r = 0.902, $P < 0.014$); on the other hand, no correlation was found between the affinity and k_{off} values ($r = -0.177$, $P <$ 0.738). To visualize the relationship between a ligand's k_{on} and k_{off} values with regard to its affinity, a kinetic map was prepared (Fig. 8D), where compounds along the same diagonal lines show similar affinities, but have different kinetic properties. For instance, SR144528 and GW405833 displayed similar K_D values (i.e., located on same diagonal), but SR144528 had a slower dissociation rate, while GW405833 compensated its fast dissociation rate with an increased receptor association rate. Taken together, the kinetic map shows that each compound possesses a characteristic kinetic profile, which is not necessarily correlated to its affinity.

TABLE 2
Affinity and kinetic binding proprieties of CB2R reference ligands determined by [^{3}H]RO6957022 displacement and competition association experiments

Compound	pK_i (K_i) (*nM*)	k_{on} (*nM^{-1}/min^{-1}*)	k_{off} (*min^{-1}*)	RT (*minute*)	K_D (*nM*)
RO6957022	8.9 ± 0.05 (1.2)	0.15 ± 0.03	0.19 ± 0.03	5.3 ± 0.7	1.3 ± 0.4
CP55,940	9.3 ± 0.03 (0.50)	0.22 ± 0.02	0.20 ± 0.02	5.0 ± 0.4	0.90 ± 0.1
JWH-133	7.4 ± 0.07 (39)	0.0042 ± 0.001	0.31 ± 0.07	3.2 ± 0.7	75 ± 24
HU-308	7.6 ± 0.08 (25)	0.011 ± 0.001	0.23 ± 0.01	4.2 ± 0.2	21 ± 3
AM1241	8.2 ± 0.03 (6.3)	—	—	—	—
GW405833	8.4 ± 0.02 (3.5)	0.25 ± 0.06	0.70 ± 0.1	1.4 ± 0.3	2.8 ± 0.8
SR144528	8.3 ± 0.02 (5.0)	0.028 ± 0.003	0.12 ± 0.02	8.7 ± 1.7	4.1 ± 0.9
AM630	7.7 ± 0.03 (20)	—	—	—	—
AEA	—	0.0024 ± 0.0004	0.73 ± 0.11	1.4 ± 0.2	305 ± 45
2-AG	—	0.032 ± 0.005	3.2 ± 0.9	0.31 ± 0.09	99 ± 27
NE	—	0.042 ± 0.033	6.3 ± 1.0	0.16 ± 0.03	151 ± 24

Receptor affinities (K_i) were calculated using the Cheng- Prusoff equation (Cheng and Prusoff, 1973). Kinetic binding parameters (i.e., k_{on} and k_{off}) were obtained using the Motulsky-Mahan model (Motulsky and Mahan, 1984). The derived affinity values were calculated using the equation $K_D = k_{off}/k_{on}$. The results shown are the mean ± S.E.M. of at least three individual experiments, em dashes indicate the absence of value for the mentioned compound.

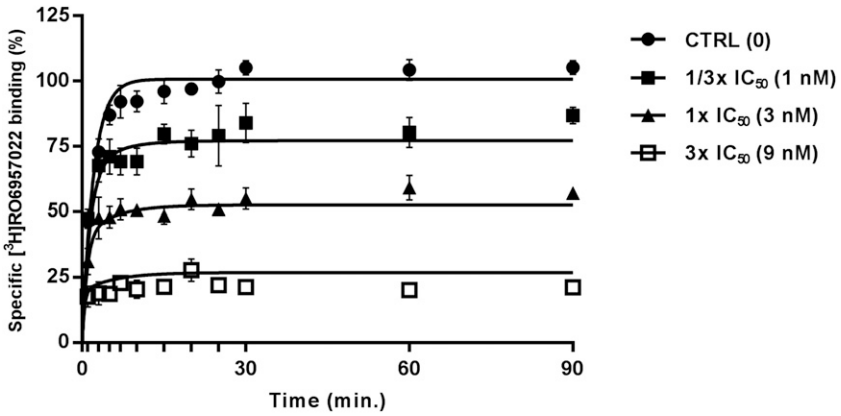

Fig. 5. Homologous competition association of [^{3}H]RO6957022. Competition association experiment of [^{3}H]RO6957022 on CHO-K1_hCB$_2$ membranes using three concentrations (0.3-, 1.0-, and 3.0-fold IC_{50}) of its unlabeled congener. Data are shown as the average and S.E.M. of seven independent experiments each performed in duplicate.

Discussion

A decade after the (re)introduction of the concept of target RT of drugs (Copeland et al., 2006) growing evidence has been accumulated on its potential implications in lead optimization when used prospectively (Guo et al., 2017). The concept behind receptor-ligand kinetics is to select candidate drugs based not only on their affinity but also by taking into account their association and dissociation rates to and from their target (Copeland et al., 2006). However, when one desires to use a compound's kinetic binding profile prospectively, kinetic binding assays are needed that often require radiolabeled or fluorescently labeled tool compounds.

In this study, we report the characterization of [^{3}H]RO6957022, a novel high-affinity radioligand with high selectivity for the human CB2R. Recently, an [^{11}C] derivative of this compound was reported as a positron emission tomography imaging probe (Slavik et al., 2015), where it was shown that reduced lipophilicity (log $D_{7.4}$ = 1.94), high CB2R affinity (K_i = 2.5 nM), and selectivity (<1000 times over hCB$_1$) with a corresponding spleen-specific biodistribution made this compound a valuable tool for in vivo positron emission tomography screenings. Another aspect that makes [^{3}H]RO6957022 a suitable tool compound for in vitro kinetic binding assays is its inverse agonistic behavior. CB2R pharmacological studies are often performed in heterologous cell lines overexpressing the receptor. In these in vitro systems, the increased receptor expression often is not accompanied by augmented G protein levels; therefore, a large part of the receptor population is in its inactive form (Gonsiorek et al., 2006). This was also true for the employed cell line (i.e., CHO-K1_hCB2), in which considerably high levels of CB2R were expressed as determined by saturation experiments (Table 1). In this scenario an inverse agonist radioligand is the preferred option for (kinetic) binding studies since the biggest receptor subpopulation is targeted, which results in a larger assay window. This concept was also experimentally tested in parallel with the prototypical probe [^{3}H]CP55,940 (Supplemental Fig. 1). Although [^{3}H]RO6957022 has lower specific activity with respect to [^{3}H]CP55,940, both radioligands displayed comparable TB signals, supporting the idea behind the use of an inverse agonist for these studies. On the other hand, NSB of [^{3}H]RO6957022 was significantly lower, as expected from its aforementioned improved features, confirming the usefulness of this new probe for filtration binding studies.

Once the [^{3}H]RO6957022 competition association assay was validated (Fig. 5), we selected representative compounds from the CB2R reference ligands, i.e., two full agonists (CP55,940 and JWH-133), a partial agonist (GW405833), and an inverse agonist (SR144528), for proof of concept. Using this [^{3}H]RO6957022 assay we were able to determine the k_{on} and k_{off} values of all tested ligands. The derived kinetic K_D values obtained from these kinetic data were highly correlated to the obtained equilibrium K_i values (Fig. 8A), confirming the consistency of the kinetic binding data obtained with [^{3}H]RO6957022. Among the tested ligands, SR144528 showed the longest residence time (RT = 8.7 ± 1.7 minutes), resulting in a characteristic but small overshoot of the competition association curve (Fig. 6). The present kinetic binding data, together with the desirable pharmacokinetic features of SR144528, could explain its long-lasting CB2R target occupancy reported in mouse spleen (Rinaldi-Carmona et al., 1998). Of note, since all measured receptor RTs are quite short (Table 2), the pharmacokinetics of these compounds is probably faster than their receptor RT, which means that the latter parameter will probably not be (solely) driving their pharmacodynamics effects in vivo (Dahl and Akerud, 2013). However, the association rate constants exhibited a substantial spread, covering more than two log units among the studied CB2R synthetic and endogenous ligands, while the dissociation rates were more similar. Furthermore, as opposed to their dissociation rate constants, the association rate constants significantly correlated with the K_i value, implying that the k_{on} value was the main driving force in CB2R affinity in the tested synthetic ligands. This is in contrast to a more common observation that target RT is the principal determinant for receptor affinity, as was reported on a number of targets, e.g., M_3 (Sykes et al., 2009) and A_{2A} (Guo et al., 2012) receptors. However, there are some reports where the influence of the k_{on} value on affinity has been described. For instance, agonists for the β_2-adrenergic receptor (Sykes and Charlton, 2012) and modulators of the K_v11.1 (hERG) channel (Yu et al., 2015a,b) showed a similar correlation between k_{on} and affinity, where a role for the lipid membrane was postulated in the β_2-adrenergic receptor. This reinforces the notion that variations in the k_{on} values can greatly impact the overall receptor affinity (de Witte et al., 2016; Vauquelin, 2016).

Considering the binding kinetic profile and physicochemical properties of the tested ligands, phenomena such as rebinding and membrane interactions should also be taken into account, since these are likely to generate so-called micro-pharmacokinetics and -dynamics in the proximity of CB2R, which can affect the kinetic binding parameters. For AEA (Tian et al., 2005) and

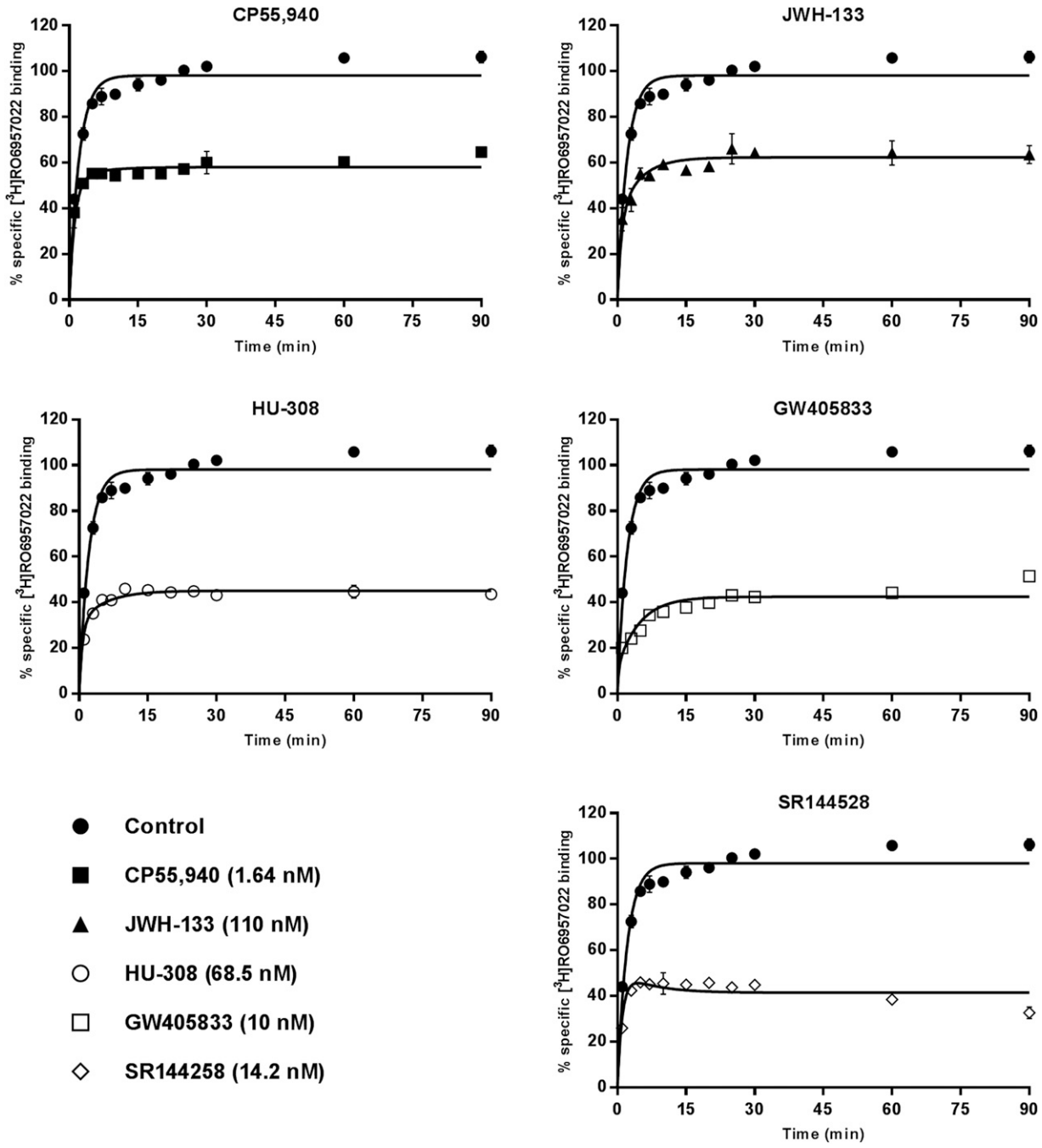

Fig. 6. Kinetic binding experiments of well-known CB_2 ligands. Competition association of [^{3}H]RO6957022 on CHO-K1_hCB_2 membranes at 25°C in either the absence (control) or presence of a single concentration (i.e., IC_{50} value) of CP55,940, JWH-133, HU-308, GW405833, or SR144528. Data are shown as the mean and S.E.M. of three independent experiments each performed in duplicate.

CP55,940 (Kimura et al., 2009), there is evidence that these ligands approach the CB2R by fast lateral diffusion from the membrane bilayer. This was substantiated in the recently published cannabinoid receptor type 1 crystal structure, in which putative lipid access from the membrane bilayer was also described (Shao et al., 2016). Similarly, for AM841 (Pei et al., 2008), a CB2R covalent agonist, and 2-AG (Hurst et al., 2010) it has been shown that these ligands first distribute in the lipid bilayer and then bind and activate the receptor within microseconds (Hurst et al., 2010). The latter fits well with the high k_{on} value of 2-AG obtained in our kinetic binding experiments.

Finally, in light of the high and dynamic endocannabinoid tone in healthy states—and especially in diseased states (Cabral and Griffin-Thomas, 2009)—the characterization of the kinetic binding behavior of these endogenous ligands can reveal important insights about the physiology of these lipid mediators. Although the assessed affinities of the three endocannabinoids were in a close range (pK_D = 6.5–7.0), significant differences were found in their kinetic binding profiles, i.e., 2-AG and NE showed a 10-fold higher k_{on} value for CB2R compared with AEA (Fig. 7; Table 2). Interestingly, their association rates appear to correlate with the described

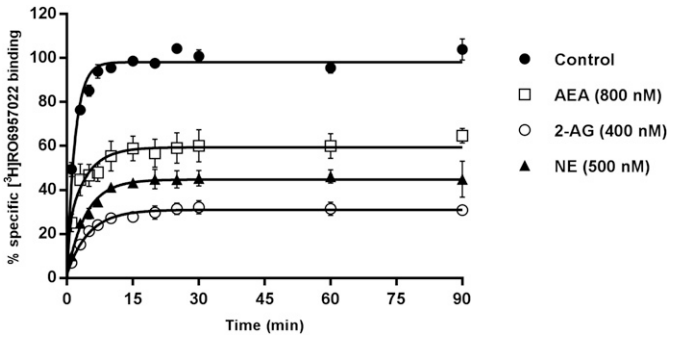

Fig. 7. Kinetic binding behavior of the endogenous ligands at the hCB_2 receptor. Competition association of [^{3}H]RO6957022 on CHO-K1_hCB_2 membranes at 25°C in either the absence (control) or presence of a single concentration (i.e., IC_{50} value) of AEA, 2-AG, or NE. Data are shown as the mean and S.E.M. of six independent experiments each performed in duplicate.

functional nature, i.e., 2-AG is a full agonist for the CB2R and AEA is a partial agonist (Gonsiorek et al., 2000; Soethoudt et al., 2017). Moreover, the obtained molecular evidence of the endocannabinoid-CB2R binding kinetics fits with the on-demand nature of the endocannabinoid system (Di Marzo, 2009), where endocannabinoids are rapidly and locally synthesized or degraded, which allows for swift receptor binding without a prolonged functional effect (Piomelli, 2003). Considering the substantial paracrine concentrations of 2-AG, together with its high k_{on} value toward CB2R, it can be speculated that this endocannabinoid will quickly achieve effective target occupancy (Schoop and Dey, 2015). Furthermore, CB2R has been reported to rapidly undergo desensitization (Bouaboula et al., 1999). With this in mind, more transient receptor activation would be favorable for an effective but safe physiologic action.

Therefore, the question arises whether a long or short RT would be most desirable for the CB2R. The short RTs of the endogenous cannabinoids (Table 2) may constitute a clue already, since knowing the binding kinetics of a target's endogenous ligands could give important information for a proper pharmacological intervention (Nederpelt et al., 2016). Likewise, the high k_{on} values and short RTs found for the synthetic ligands in Table 2 are reminiscent of what has already been described for other molecular targets (Copeland, 2010), in which a pulse (i.e., fast k_{on} and k_{off}) rather than sustained target occupancy by an antagonist is beneficial in achieving desirable pharmacological outcomes and reduced side effects. An example of the latter is the dopamine D_2 receptor (Pan et al., 2008). For this target a positive correlation was found between extrapyramidal side effects and prolonged receptor blockade by long RT antagonists (Seeman, 2005), possibly due to the continued

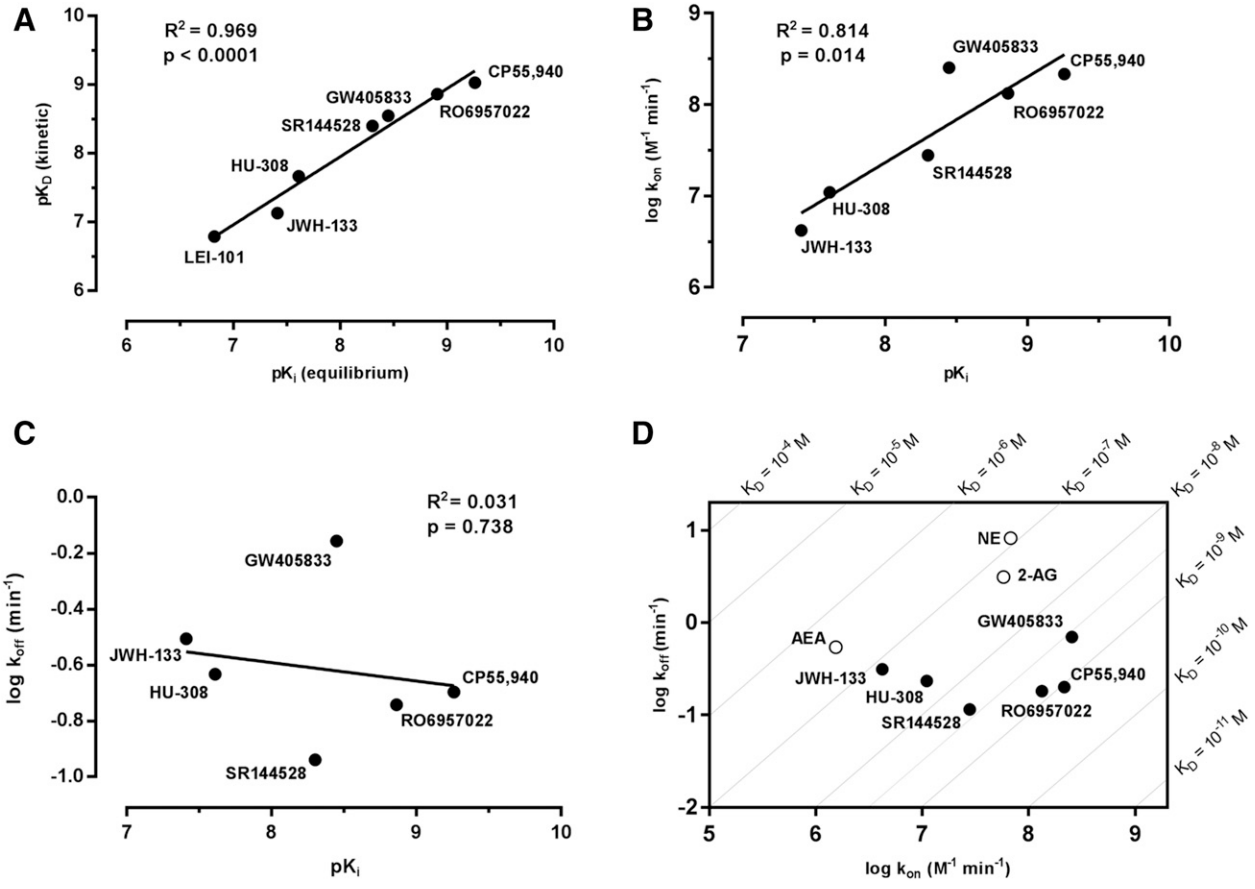

Fig. 8. Correlation plots of equilibrium and kinetic parameters of reference CB_2 ligands. (A) Negative logarithmic transformation of affinities determined by equilibrium displacement (pK_i) versus kinetic binding (pK_D). (B) Correlation between logarithmic association rate [$\log k_{on}$ (M^{-1}/min^{-1})] and pK_i. (C) Correlation between logarithmic dissociation rate [$\log k_{off}$(min^{-1})] and pK_i. (D) Kinetic map in which the k_{on} values are plotted against the k_{off} values. Gray diagonal lines indicate an identical affinity (K_D) value for different k_{off}/k_{on} combinations. Data are shown as the average values from Table 2 without error bars to provide clarity.

suppression of the subcortical dopaminergic activity (Casey, 2004). Analogously, pharmacological interventions on CB2R should consider the local mediator function of endocannabinoids (Di Marzo, 2008) in physiology and their pivotal role in immunomodulation. Specifically, CB2R activation triggers a complex signal cascade that can either reduce the early phases of the immune response (Herring et al., 1998) through inhibition of adenylyl cyclase or induce immunosuppression through apoptosis mechanisms (Eisenstein et al., 2007). To date, the inhibitory effects of cannabinoids on the immune system are known to be transient (Pandey et al., 2009), allowing the immune response to be quickly restored for potential infectious threats. Therefore, although speculative, long RT CB2R agonists as well as antagonists would not be desirable, since they would continuously interfere with endocannabinoid system homeostasis, ultimately leading to adverse effects.

Conclusions

We have characterized a novel, high-affinity inverse agonist radioligand for human CB2R, the 2,5,6-substituted pyridine derivative [^{3}H]RO695702. Its CB2R binding properties have been validated in equilibrium saturation and displacement assays, as well as kinetically in (competition) association and dissociation assays. Using a variety of CB2R reference ligands, we showed that [^{3}H]RO6957022 is an excellent tool compound to determine ligand affinities and kinetic rate constants at CB2R, including (for the first time) the kinetic binding profiles of the CB2R endogenous ligands. The latter gives important insights into the mechanism of action for these mediators of such paramount lipid signaling. This improved knowledge of endocannabinoid system physiology can be translated into a better therapeutic drug design strategy. Thus, with the introduction of [^{3}H]RO6957022 we hope to aid and stimulate the development and kinetic optimization of ligands for CB2R in early drug discovery.

Acknowledgments

The authors thank Mathias Müller for the contribution to the synthesis of [^{3}H]RO6957022.

Authorship Contributions

Participated in research design: Martella, Rufer, Grether, Fingerle, Ullmer, IJzerman, van der Stelt, Heitman.

Conducted experiments: Martella, Sijben.

Contributed new reagents or analytic tools: Grether, Hartung, van der Stelt.

Performed data analysis: Martella, Sijben, Rufer.

Wrote or contributed to the writing of the manuscript: Martella, Rufer, Grether, Fingerle, Ullmer, IJzerman, van der Stelt, Heitman.

References

Anand P, Whiteside G, Fowler CJ, and Hohmann AG (2009) Targeting CB_2 receptors and the endocannabinoid system for the treatment of pain. *Brain Res Brain Res Rev* **60**:255–266.

Aso E, Juvés S, Maldonado R, and Ferrer I (2013) CB_2 cannabinoid receptor agonist ameliorates Alzheimer-like phenotype in AβPP/PS1 mice. *J Alzheimers Dis* **35**: 847–858.

Benesty J, Chen J, Huang Y, and Cohen I (2009) Pearson correlation coefficient, in *Noise Reduction in Speech Processing* pp 1–4, Springer, Berlin.

Bouaboula M, Dussossoy D, and Casellas P (1999) Regulation of peripheral cannabinoid receptor CB_2 phosphorylation by the inverse agonist SR 144528. Implications for receptor biological responses. *J Biol Chem* **274**:20397–20405.

Brown SM, Wager-Miller J, and Mackie K (2002) Cloning and molecular characterization of the rat CB2 cannabinoid receptor. *Biochim Biophys Acta* **1576**:255–264.

Cabral GA and Griffin-Thomas L (2009) Emerging role of the CB_2 cannabinoid receptor in immune regulation and therapeutic prospects. *Expert Rev Mol Med* **11**:e3.

Cabral GA, Raborn ES, Griffin L, Dennis J, and Marciano-Cabral F (2008) CB_2 receptors in the brain: role in central immune function. *Br J Pharmacol* **153**: 240–251.

Casey DE (2004) Pathophysiology of antipsychotic drug-induced movement disorders. *J Clin Psychiatry* **65** (**Suppl 9**):25–28.

Cheng Y and Prusoff WH (1973) Relationship between the inhibition constant (K_I) and the concentration of inhibitor which causes 50 per cent inhibition (I_{50}) of an enzymatic reaction. *Biochem Pharmacol* **22**:3099–3108.

Copeland RA (2010) The dynamics of drug-target interactions: drug-target residence time and its impact on efficacy and safety. *Expert Opin Drug Discov* **5**:305–310.

Copeland RA, Pompliano DL, and Meek TD (2006) Drug-target residence time and its implications for lead optimization. *Nat Rev Drug Discov* **5**:730–739.

Dahl G and Akerud T (2013) Pharmacokinetics and the drug-target residence time concept. *Drug Discov Today* **18**:697–707.

Devane WA, Dysarz FA, III, Johnson MR, Melvin LS, and Howlett AC (1988) Determination and characterization of a cannabinoid receptor in rat brain. *Mol Pharmacol* **34**:605–613.

de Witte WEA, Danhof M, van der Graaf PH, and de Lange ECM (2016) In vivo target residence time and kinetic selectivity: the association rate constant as determinant. *Trends Pharmacol Sci* **37**:831–842.

Dhopeshwarkar A and Mackie K (2014) CB_2 Cannabinoid receptors as a therapeutic target—what does the future hold? *Mol Pharmacol* **86**:430–437.

Di Marzo V (2008) Targeting the endocannabinoid system: to enhance or reduce? *Nat Rev Drug Discov* **7**:438–455.

Di Marzo V (2009) The endocannabinoid system: its general strategy of action, tools for its pharmacological manipulation and potential therapeutic exploitation. *Pharmacol Res* **60**:77–84.

Di Marzo V and Fontana A (1995) Anandamide, an endogenous cannabinomimetic eicosanoid: 'killing two birds with one stone'. *Prostaglandins Leukot Essent Fatty Acids* **53**:1–11.

Eisenstein TK, Meissler JJ, Wilson Q, Gaughan JP, and Adler MW (2007) Anandamide and Δ^9-tetrahydrocannabinol directly inhibit cells of the immune system via CB_2 receptors. *J Neuroimmunol* **189**:17–22.

Fernández-Ruiz J, Moreno-Martet M, Rodríguez-Cueto C, Palomo-Garo C, Gómez-Cañas M, Valdeolivas S, Guaza C, Romero J, Guzmán M, Mechoulam R, et al. (2011) Prospects for cannabinoid therapies in basal ganglia disorders. *Br J Pharmacol* **163**: 1365–1378.

Galiègue S, Mary S, Marchand J, Dussossoy D, Carrière D, Carayon P, Bouaboula M, Shire D, Le Fur G, and Casellas P (1995) Expression of central and peripheral cannabinoid receptors in human immune tissues and leukocyte subpopulations. *Eur J Biochem* **232**:54–61.

Gaoni Y and Mechoulam R (1964) Isolation, structure, and partial synthesis of an active constituent of hashish. *J Am Chem Soc* **86**:1646–1647.

Gonsiorek W, Hesk D, Chen SC, Kinsley D, Fine JS, Jackson JV, Bober LA, Deno G, Bian H, Fossetta J, et al. (2006) Characterization of peripheral human cannabinoid receptor (hCB2) expression and pharmacology using a novel radioligand, [^{35}S]Sch225336. *J Biol Chem* **281**:28143–28151.

Gonsiorek W, Lunn C, Fan X, Narula S, Lundell D, and Hipkin RW (2000) Endocannabinoid 2-arachidonyl glycerol is a full agonist through human type 2 cannabinoid receptor: antagonism by anandamide. *Mol Pharmacol* **57**:1045–1050.

Guindon J and Hohmann AG (2008) Cannabinoid CB_2 receptors: a therapeutic target for the treatment of inflammatory and neuropathic pain. *Br J Pharmacol* **153**:319–334.

Guo D, Heitman LH, and IJzerman AP (2017) Kinetic aspects of the interaction between ligand and G protein-coupled receptor: the case of the adenosine receptors. *Chem Rev* **117**:38–66.

Guo D, Mulder-Krieger T, IJzerman AP, and Heitman LH (2012) Functional efficacy of adenosine A_2A receptor agonists is positively correlated to their receptor residence time. *Br J Pharmacol* **166**:1846–1859.

Herring AC, Koh WS, and Kaminski NE (1998) Inhibition of the cyclic AMP signaling cascade and nuclear factor binding to CRE and κB elements by cannabinol, a minimally CNS-active cannabinoid. *Biochem Pharmacol* **55**:1013–1023.

Horváth B, Magid L, Mukhopadhyay P, Bátkai S, Rajesh M, Park O, Tanchian G, Gao RY, Goodfellow CE, Glass M, et al. (2012) A new cannabinoid CB_2 receptor agonist HU-910 attenuates oxidative stress, inflammation and cell death associated with hepatic ischaemia/reperfusion injury. *Br J Pharmacol* **165**:2462–2478.

Hurst DP, Grossfield A, Lynch DL, Feller S, Romo TD, Gawrisch K, Pitman MC, and Reggio PH (2010) A lipid pathway for ligand binding is necessary for a cannabinoid G protein-coupled receptor. *J Biol Chem* **285**:17954–17964.

Kimura T, Cheng K, Rice KC, and Gawrisch K (2009) Location, structure, and dynamics of the synthetic cannabinoid ligand CP-55,940 in lipid bilayers. *Biophys J* **96**:4916–4924.

Li Q, Wang F, Zhang YM, Zhou JJ, and Zhang Y (2013) Activation of cannabinoid type 2 receptor by JWH133 protects heart against ischemia/reperfusion-induced apoptosis. *Cell Physiol Biochem* **31**:693–702.

Ligresti A, De Petrocellis L, and Di Marzo V (2016) From phytocannabinoids to cannabinoid receptors and endocannabinoids: pleiotropic physiological and pathological roles through complex pharmacology. *Physiol Rev* **96**:1593–1659.

Lotersztajn S, Teixeira-Clerc F, Julien B, Deveaux V, Ichigotani Y, Manin S, Tran-Van-Nhieu J, Karsak M, Zimmer A, and Mallat A (2008) CB2 receptors as new therapeutic targets for liver diseases. *Br J Pharmacol* **153**:286–289.

Ludden TM, Beal SL, and Sheiner LB (1994) Comparison of the akaike information criterion, the Schwarz criterion and the F test as guides to model selection. *J Pharmacokinet Biopharm* **22**:431–445.

Mechoulam R, Hanuš LO, Pertwee R, and Howlett AC (2014) Early phytocannabinoid chemistry to endocannabinoids and beyond. *Nat Rev Neurosci* **15**:757–764.

Morales P, Hernandez-Folgado L, Goya P, and Jagerovic N (2016) Cannabinoid receptor 2 (CB_2) agonists and antagonists: a patent update. *Expert Opin Ther Pat* **26**: 843–856.

Moris D, Georgopoulos S, Felekouras E, Patsouris E, and Theocharis S (2015) The effect of endocannabinoid system in ischemia-reperfusion injury: a friend or a foe? *Expert Opin Ther Targets* **19**:1261–1275.

Motulsky HJ and Mahan LC (1984) The kinetics of competitive radioligand binding predicted by the law of mass action. *Mol Pharmacol* **25**:1–9.
Mukhopadhyay P, Baggelaar M, Erdelyi K, Cao Z, Cinar R, Fezza F, Ignatowska-Janlowska B, Wilkerson J, van Gils N, Hansen T, et al. (2016) The novel, orally available and peripherally restricted selective cannabinoid CB_2 receptor agonist LEI-101 prevents cisplatin-induced nephrotoxicity. *Br J Pharmacol* **173**:446–458.
Mukhopadhyay P, Rajesh M, Pan H, Patel V, Mukhopadhyay B, Bátkai S, Gao B, Haskó G, and Pacher P (2010) Cannabinoid-2 receptor limits inflammation, oxidative/nitrosative stress, and cell death in nephropathy. *Free Radic Biol Med* **48**:457–467.
Munro S, Thomas KL, and Abu-Shaar M (1993) Molecular characterization of a peripheral receptor for cannabinoids. *Nature* **365**:61–65.
Nederpelt I, Bleeker D, Tuijt B, IJzerman AP, and Heitman LH (2016) Kinetic binding and activation profiles of endogenous tachykinins targeting the NK1 receptor. *Biochem Pharmacol* **118**:88–95.
Ofek O, Karsak M, Leclerc N, Fogel M, Frenkel B, Wright K, Tam J, Attar-Namdar M, Kram V, Shohami E, et al. (2006) Peripheral cannabinoid receptor, CB2, regulates bone mass. *Proc Natl Acad Sci USA* **103**:696–701.
Pan B, Hillard CJ, and Liu QS (2008) D2 dopamine receptor activation facilitates endocannabinoid-mediated long-term synaptic depression of GABAergic synaptic transmission in midbrain dopamine neurons via cAMP-protein kinase A signaling. *J Neurosci* **28**:14018–14030.
Pandey R, Mousawy K, Nagarkatti M, and Nagarkatti P (2009) Endocannabinoids and immune regulation. *Pharmacol Res* **60**:85–92.
Pei Y, Mercier RW, Anday JK, Thakur GA, Zvonok AM, Hurst D, Reggio PH, Janero DR, and Makriyannis A (2008) Ligand-binding architecture of human CB2 cannabinoid receptor: evidence for receptor subtype-specific binding motif and modeling GPCR activation. *Chem Biol* **15**:1207–1219.
Picone RP and Kendall DA (2015) Minireview: from the bench, toward the clinic: therapeutic opportunities for cannabinoid receptor modulation. *Mol Endocrinol* **29**:801–813.
Piomelli D (2003) The molecular logic of endocannabinoid signalling. *Nat Rev Neurosci* **4**:873–884.
Riether D (2012) Selective cannabinoid receptor 2 modulators: a patent review 2009–present. *Expert Opin Ther Pat* **22**:495–510.
Rinaldi-Carmona M, Barth F, Millan J, Derocq JM, Casellas P, Congy C, Oustric D, Sarran M, Bouaboula M, Calandra B, et al. (1998) SR 144528, the first potent and selective antagonist of the CB2 cannabinoid receptor. *J Pharmacol Exp Ther* **284**:644–650.
Schoop A and Dey F (2015) On-rate based optimization of structure-kinetic relationship—surfing the kinetic map. *Drug Discov Today Technol* **17**:9–15.
Seeman P (2005) An update of fast-off dopamine D_2 atypical antipsychotics. *Am J Psychiatry* **162**:1984–1985.
Shao Z, Yin J, Chapman K, Grzemska M, Clark L, Wang J, and Rosenbaum DM (2016) High-resolution crystal structure of the human CB1 cannabinoid receptor. *Nature* **540**:602–606.
Slavik R, Grether U, Müller Herde A, Gobbi L, Fingerle J, Ullmer C, Krämer SD, Schibli R, Mu L, and Ametamey SM (2015) Discovery of a high affinity and selective pyridine analog as a potential positron emission tomography imaging agent for cannabinoid type 2 receptor. *J Med Chem* **58**:4266–4277.
Smith PK, Krohn RI, Hermanson GT, Mallia AK, Gartner FH, Provenzano MD, Fujimoto EK, Goeke NM, Olson BJ, and Klenk DC (1985) Measurement of protein using bicinchoninic acid. *Anal Biochem* **150**:76–85.
Soethoudt M, Grether U, Fingerle J, Grim TW, Fezza F, de Petrocellis L, Ullmer C, Rothenhäusler B, Perret C, van Gils N, et al. (2017) Cannabinoid CB_2 receptor ligand profiling reveals biased signalling and off-target activity. *Nat Commun* **8**:13958.
Sykes DA and Charlton SJ (2012) Slow receptor dissociation is not a key factor in the duration of action of inhaled long-acting β2-adrenoceptor agonists. *Br J Pharmacol* **165**:2672–2683.
Sykes DA, Dowling MR, and Charlton SJ (2009) Exploring the mechanism of agonist efficacy: a relationship between efficacy and agonist dissociation rate at the muscarinic M_3 receptor. *Mol Pharmacol* **76**:543–551.
Sykes DA, Parry C, Reilly J, Wright P, Fairhurst RA, and Charlton SJ (2014) Observed drug-receptor association rates are governed by membrane affinity: the importance of establishing "micro-pharmacokinetic/pharmacodynamic relationships" at the β_2-adrenoceptor. *Mol Pharmacol* **85**:608–617.
Tian X, Guo J, Yao F, Yang DP, and Makriyannis A (2005) The conformation, location, and dynamic properties of the endocannabinoid ligand anandamide in a membrane bilayer. *J Biol Chem* **280**:29788–29795.
Tummino PJ and Copeland RA (2008) Residence time of receptor-ligand complexes and its effect on biological function. *Biochemistry* **47**:5481–5492.
Turcotte C, Blanchet MR, Laviolette M, and Flamand N (2016) The CB_2 receptor and its role as a regulator of inflammation. *Cell Mol Life Sci* **73**:4449–4470.
Vauquelin G (2016) Effects of target binding kinetics on in vivo drug efficacy: k_{off}, k_{on} and rebinding. *Br J Pharmacol* **173**:2319–2334.
Yu Z, IJzerman AP, and Heitman LH (2015a) K_v 11.1 (hERG)-induced cardiotoxicity: a molecular insight from a binding kinetics study of prototypical K_v 11.1 (hERG) inhibitors. *Br J Pharmacol* **172**:940–955.
Yu Z, van Veldhoven JPD, Louvel J, 't Hart IME, Rook MB, van der Heyden MAG, Heitman LH, and IJzerman AP (2015b) Structure-affinity relationships (SARs) and structure-kinetics relationships (SKRs) of K_v11.1 blockers. *J Med Chem* **58**:5916–5929.

Address correspondence to: Dr. Laura H. Heitman, Molecular Pharmacology, Leiden Academic Centre for Drug Research, Leiden University, Einsteinweg 55, 2333 CC Leiden, The Netherlands. E-mail: l.h.heitman@lacdr.leidenuniv.nl